Evaluation and Hydrological Application of CMADS Reanalysis Precipitation Data against Four Satellite Precipitation Products in the Upper Huaihe River Basin, China

Shanhu JIANG[1], Ruolan LIU[1], Liliang REN[1*], Menghao WANG[1], Junchao SHI[2], Feng ZHONG[1], and Zheng DUAN[3]

1 *State Key Laboratory of Hydrology-Water Resources and Hydraulic Engineering*, *Hohai University*, *Nanjing* 210098, *China*
2 *Hydrology and Water Resources Monitoring and Forecasting Center*, *Ministry of Water Resources*, *Beijing* 100053, *China*
3 *Department of Physical Geography and Ecosystem Science*, *Lund University*, *Lund* S-22362, *Sweden*

(Received February 9, 2020; in final form May 28, 2020)

ABSTRACT

Satellite- and reanalysis-based precipitation products are important data source for precipitation, particularly in areas with a sparse gauge network. Here, five open-access precipitation products, including the newly released China Meteorological Assimilation Driving Datasets for the Soil and Water Assessment Tool (SWAT) model (CMADS) reanalysis dataset and four widely used bias-adjusted satellite precipitation products [SPPs; i.e., Tropical Rainfall Measuring Mission (TRMM) Multisatellite Precipitation Analysis 3B42 Version 7 (TMPA 3B42V7), Climate Prediction Center (CPC) morphing technique satellite–gauge blended product (CMORPH-BLD), Climate Hazards Group Infrared Precipitation with Station Data (CHIRPS), and Precipitation Estimation from Remotely Sensed Information using Artificial Neural Networks–Climate Data Record (PERSIANN-CDR)], were assessed. These products were first compared with the gauge observed data collected for the upper Huaihe River basin, and then were used as forcing data for streamflow simulation by the Xin'anjiang (XAJ) hydrological model under two scenarios with different calibration procedures. The performance of CMADS precipitation product for the Chinese mainland was also assessed. The results show that: (1) for the statistical assessment, CMADS and CMORPH-BLD perform the best, followed by TMPA 3B42V7, CHIRPS, and PERSIANN-CDR, among which the correlation coefficient (CC) and root-mean-square error (RMSE) values of CMADS are optimal, although it exhibits certain significant negative relative bias (BIAS; −22.72%); (2) CMORPH-BLD performs the best in capturing and detecting rainfall events, while CMADS tends to underestimate heavy and torrential precipitation; (3) for streamflow simulation, the performance of using CMADS as input is very good, with the highest Nash–Sutcliffe efficiency (NSE) values (0.85 and 0.75 for calibration period and validation period, respectively); and (4) CMADS exhibits high accuracy in eastern China while with significant negative BIAS, and the performance declines from southeast to northwest. The statistical and hydrological evaluations show that CMADS and CMORPH-BLD have high potential for observing precipitation. As high negative BIAS values showed up in CMADS evaluation, further study on the error sources from original data and calibration algorithms is necessary. This study can serve as a reference for selecting precipitation products in data-scarce regions with similar climates and topography in the Global Precipitation Measurement (GPM) era.

Key words: reanalysis precipitation data, China Meteorological Assimilation Driving Datasets for the Soil and Water Assessment Tool (SWAT) model (CMADS), satellite precipitation, hydrological evaluation, Xin'anjiang (XAJ) hydrological model

Citation: Jiang, S. H., R. L. Liu, L. L. Ren, et al., 2020: Evaluation and hydrological application of CMADS reanalysis precipitation data against four satellite precipitation products in the upper Huaihe River basin, China. *J. Meteor. Res.*, **34**(5), 1096–1113, doi: 10.1007/s13351-020-0026-6.

1. Introduction

As a primary source of water resource on earth, precipitation plays a significant part in driving global energy and hydrological cycles (Hou et al., 2014; Maggioni et al., 2016; Skofronick-Jackson et al., 2017). Accurate precipitation data are crucial for water resources management, flood forecasting, and drought monitoring

Supported by the National Key Research and Development Program of China (2016YFA0601504), National Natural Science Foundation of China (51979069), Fundamental Research Funds for the Central Universities (B200204029), and Program of Introducing Talents of Discipline to Universities by the Ministry of Education and State Administration of Foreign Experts Affairs, China (B08048).

*Corresponding author: njRLL9999@126.com.

(Jiang et al., 2012, 2014; Wu et al., 2014; Sahoo et al., 2015; Guo et al., 2016; Maggioni and Massari, 2018; Zhong et al., 2019). Therefore, accurate and reliable globally covered precipitation records must be obtained in time. At present, there are three main ways to obtain precipitation datasets including observed gauge precipitation, satellite-related precipitation retrievals, and reanalysis precipitation datasets (Sun et al., 2018), in which rain gauge observations provide relative reliable precipitation data. However, as the sparseness and unevenness of rain gauges in some regions, and rain gauge precipitation exhibits high spatial heterogeneity, constant and accurate precipitation records cannot always be obtained. As such, satellite precipitation products (SPPs) and reanalysis precipitation datasets have been widely used owing to their high spatiotemporal resolution and wide cover range, and they are open access (Seyyedi et al., 2015; Duan et al., 2019; Zhu et al., 2019).

During the past 20 years, a number of SPPs, including the Tropical Rainfall Measuring Mission (TRMM) Multisatellite Precipitation Analysis (TMPA; Huffman et al., 2007), Climate Prediction Center (CPC) morphing technique product (CMORPH; Joyce et al., 2004), Climate Hazards Group Infrared Precipitation (CHIRP; Funk et al., 2015), and Precipitation Estimation from Remotely Sensed Information using Artificial Neural Networks (PERSIANN; Sorooshian et al., 2000), have been operationally available. These SPPs were widely applied in hydrology and water resources research, and had great potential for streamflow simulation, flood frequency analysis, and extreme events monitoring at various regions, particularly for the bias-adjusted post-real-time products, including TMPA 3B42 Version 7 (TMPA 3B42V7), the CMORPH satellite–gauge blended product (CMORPH-BLD), CHIRP with Station Data (CHIRPS), and PERSIANN–Climate Data Record (PERSIANN-CDR; Golian et al., 2015; Tan et al., 2015; Duan et al., 2016; Gao et al., 2017; Su et al., 2017; Jiang et al., 2018a; Wu et al., 2018; Zhang et al., 2018; Chen et al., 2019; Golian et al., 2019; Lai et al., 2019; Sulugodu and Deka, 2019; Zhang et al., 2019). Duan et al. (2016) evaluated eight high-spatial-resolution gridded precipitation products over Adige Basin in Italy, and concluded that the CHIRPS, TMPA 3B42V7, and CMORPH-BLD performed best. Su et al. (2017) assessed the applicability of four satellite–gauge combined precipitation products for predicting extreme precipitation and streamflow over the upper Yellow River basin, China, and pointed out that CMORPH-BLD agreed best with the gauge observations, and the simulated streamflow was comparable to the gauge-based result. Maggioni and Massari (2018) summarized previous studies using SPPs for riverine flood modeling and highlighted that SPPs have significant potential in flood forecasting, and precipitation bias correction and model recalibration were two viable options to improve SPP-forced streamflow simulations.

As SPPs are estimated by calibrated infrared (IR), microwave (MW), and IR measurements, and limited gauge observations, they inevitably contain errors caused by retrieval algorithms, the measurement technologies, and calibration processes (Yong et al., 2016; Gebregiorgis et al., 2018). Supplementary reanalysis datasets are developed by combining remote sensing products, climate model outputs, and observed data (Sun et al., 2018). Nowadays, many reanalysis datasets are available, such as the ECMWF Interim Re-Analysis (ERA-Interim), the NASA Modern-Era Retrospective Analysis for Research and Applications (MERRA), and the NCEP Climate Forecast System Reanalysis (CFSR), and the number of such reanalysis datasets is still increasing (Saha et al., 2010; Dee et al., 2011; Gelaro et al., 2017). It is worthwhile mentioning that the China Meteorological Assimilation Driving Datasets for the Soil and Water Assessment Tool (SWAT) model (CMADS) over East Asia was recently developed by using the Space–Time Multiscale Analysis System (STMAS), large nested loop data, resampling, and bilinear interpolation methods (Meng and Wang, 2017; Meng et al., 2018). The CMADS precipitation data used CMORPH as the background and merged it with rain gauge data from over 30,000 automatic weather stations located in China. Several studies demonstrated that the latest CMADS precipitation product performs satisfactorily compared to in situ measurements, and can be an alternative option for obtaining precipitation information (Gao et al., 2018; Guo et al., 2018; Liu et al., 2018; Vu et al., 2018; Zhao et al., 2018; Li et al., 2019; Wang et al., 2020). For instance, Gao et al. (2018) evaluated the hydrological application of CMADS against TMPA 3B42V7, NCEP-CFSR, and PERSIANN-CDR over Xiang River basin in China, and concluded that the CMADS and TMPA 3B42V7 simulated streamflow well. Although CMADS precipitation data have been widely evaluated, the performances are inconsistent in different regions. Meanwhile, as CMADS precipitation record is based on the CMORPH SPP, it should be comprehensively compared to TRMM/Global Precipitation Measurement (GPM)-era commonly used SPPs (particularly the CMORPH-BLD product) to analyze the superiority of CMADS for merging rain gauge data.

In this study, five open-access precipitation products, including the newly released reanalysis precipitation dataset (CMADS) and four TRMM/GPM-era commonly

used bias-adjusted SPPs (TMPA 3B42V7, CMORPH-BLD, CHIRPS, and PERSIANN-CDR), were assessed. We aim to evaluate the applicability of the five precipitation products over upper Huaihe River basin in China during 2008–2015, and then further analyze the error characteristics of CMADS over the Chinese mainland. The findings can serve as a reference for selecting suitable open-access precipitation datasets for hydrological applications and help to improve future versions of the CMADS precipitation product.

2. Study area and data

2.1 *Study area*

The Xixian Basin, located in the southwestern part of the Huaihe River basin, extending from 31.5°N to 32.75°N and from 113.25°E to 115°E, has an area of 10,191 km^2 above the Xixian Hydrological Station (Fig. 1). Western and southern edge of the basin are mountainous areas, and low depressed landforms are in downstream, with elevations ranging from 33 to 1110 m. Cropland (41.8%), woodland (38.8%), paddy field (17.2%), grassland (0.54%), and water (1.32%) are the main types of land-use in the basin (Shi et al., 2011). The basin is experiencing average annual precipitation and runoff of 1145 and 371 mm, respectively. As it is affected by the East Asian monsoon in the flood season, precipitation occurs mainly between June and September. The frequent heavy rain increases the risk of flooding, thus, the hydrological application of SPPs in this basin should be assessed (Jiang et al., 2018a).

2.2 *Reanalysis and SPPs*

CMADS is a reanalysis dataset that was developed by using assimilation techniques and processing methods (Meng and Wang, 2017; Meng et al., 2018). To meet the demands for various scientific research and guarantee the reanalysis data with high resolution and high quality, CMADS includes temperature, humidity, solar radiation, wind speed, precipitation, and other variables. Using the CMORPH product as the background field, the CMADS precipitation data for China incorporate the hourly merged precipitation product from the China National Meteorological Information Center. CMADS covers the area of 0°–65°N and 60°–160°E. The CMADS precipitation product with spatiotemporal resolutions of 0.25° and 24 h covering the period of 2008–2015 was used in this study.

Launched by NASA and the Japan Aerospace Exploration Agency in 1997, the TRMM was designed to monitor tropical rainfall. The TMPA, one of the products of the TRMM, was generated from combining passive MW and IR observations (Huffman et al., 2007). The post-real-time TMPA 3B42V7 product, which is available for 50°S–50°N, covers the period of 1998–2015, and provides of 0.25° and 3 h for spatial and temporal resolution. By incorporating the Global Precipitation Climatology Center (GPCC) monthly precipitation data through inverse-error-variance weighting method for bias adjustment, TMPA 3B42V7 has performed well in many precipitation and hydrological utility research (Yong et al., 2010; Xue et al., 2013; Yuan et al., 2017).

The CMORPH product is estimated by the NOAA CPC morphing technique (Joyce et al., 2004). CMORPH Version 1.0, which is the most recent version, includes three products. Raw CMORPH (CMORPH-RAW), only estimated from satellite precipitation, was generated by both passive MW observations and IR data from low-orbit and multiple geostationary satellites, respectively. Bias-corrected CMORPH (CMORPH-CRT) is developed based on the CMORPH-RAW product but using the probability density function (PDF) to adjust the bias. The gauge–SPP, CMORPH-BLD, was outputted based on the CMORPH-CRT product merged with CPC unified daily gauges following an optimal interpolation (OI) method. All three CMORPH products that begin in 1998 are available within 60°S–60°N. Here, the CMORPH-BLD with spatiotemporal resolutions of 0.25° and 24 h, providing data from 2008 to 2015, was employed and evaluated.

CHIRPS is a merged satellite–gauge product that uses the following sources: Climate Hazards Group Precipitation Climatology (CHPClim), geostationary thermal IR satellite observations from both the CPC IR and National Climatic Data Center (NCDC) B1 IR, the TRMM 3B42 product, the rainfall fields of the atmospheric model from the NOAA Climate Forecast System Version 2 (CFSv2), and the gauge observations from multiple sources (Funk et al., 2015). Released in early 2014, CHIRPS has a relatively high spatial resolution of 0.05°, covers the 50°S–50°N region, and provides rainfall data from 1981 to present.

PERSIANN-CDR provides precipitation data with spatiotemporal resolutions of 0.25° and 24 h from 1983 to present, and covers the area between 60°S and 60°N (Sorooshian et al., 2000). An artificial neural network (ANN) model was used to convert IR observations from geostationary satellite imagery into precipitation rates. The Stage-IV precipitation data from the NCEP were used for the initial training of the ANN model, and its parameters remained fixed during the running period. The GridSat-B1 data were used as input for precipitation,

producing PERSIANN B1, which was further calibrated by using the monthly Global Precipitation Climatology Project (GPCP) data to reduce bias (Table 1).

2.3 *Gauge precipitation data*

Daily precipitation data were obtained from 22 densely distributed rain gauge stations in the Xixian Basin (Fig. 1). The daily streamflow data for the Xixian Hydrological Station and meteorological data for the Xinyang Station were both collected from the Hydrological Bureau of the Ministry of Water Resources of China. The rain gauge data were converted into spatially distributed precipitation data following the inverse distance weighting interpolation method (Bartier and Keller, 1996). The digital elevation model (DEM) data with a spatial resolution of 30 arc s used in this study were obtained from the U.S. Geological Survey. The vegetation-type data were collected from the Moderate Resolution Imaging Spectroradiometer land cover data using the International Geosphere–Biosphere Program classification system (Friedl et al., 2002).

3. Methodology

3.1 *The Xin'anjiang (XAJ) model*

Developed by Zhao (1992) in late 1970s, the XAJ model is a renowned hydrological model and has been broadly applied to simulate streamflow, evaluate water resources, and design hydrological station networks in humid and semiarid watersheds throughout China (Zhao, 1992; Xu et al., 2016; Jiang et al., 2018b). A grid-based XAJ model was used in this study, which uses the saturation excess runoff scheme to compute total runoff of every single grid, and then divides the streamflow into surface runoff, interflow, and groundwater flow. The overland flow concentration is calculated by the flow direction within the grid, and the river network flow concentration is then computed to simulate streamflow. The model contains 16 parameters and their numeric ranges and default values are shown in Section 4.3. Several model parameters are very sensitive and need to be calibrated (Zhao, 1992; Yuan et al., 2019). For instance, the

Table 1. Summary of the precipitation datasets used in this study

Full name and details	Abbreviation	Coverage	Spatiotemporal resolution used	Data source
China Meteorological Assimilation Driving Datasets for the SWAT model Version 1.1	CMADS	0°–65°N, 60°–160°E	Daily, 0.25°	http://www.cmads.org/
Tropical Rainfall Measuring Mission Multisatellite Precipitation Analysis 3B42 Version 7	TMPA 3B42V7	50°S–50°N	Daily, 0.25°	https://mirador.gsfc.nasa.gov/
Climate Prediction Center morphing technique satellite–gauge blended product	CMORPH-BLD	60°S–60°N	Daily, 0.25°	ftp://ftp.cpc.ncep.noaa.gov/precip/CMORPH_V1.0/
Climate Hazards Group Infrared Precipitation with Station Data Version 2.0	CHIRPS	50°S–50°N	Daily, 0.05°	http://chg.geog.ucsb.edu/data/chirps/
Precipitation Estimation from Remotely Sensed Information using Artificial Neural Networks–Climate Data Record	PERSIANN-CDR	60°S–60°N	Daily, 0.25°	http://chrsdata.eng.uci.edu/

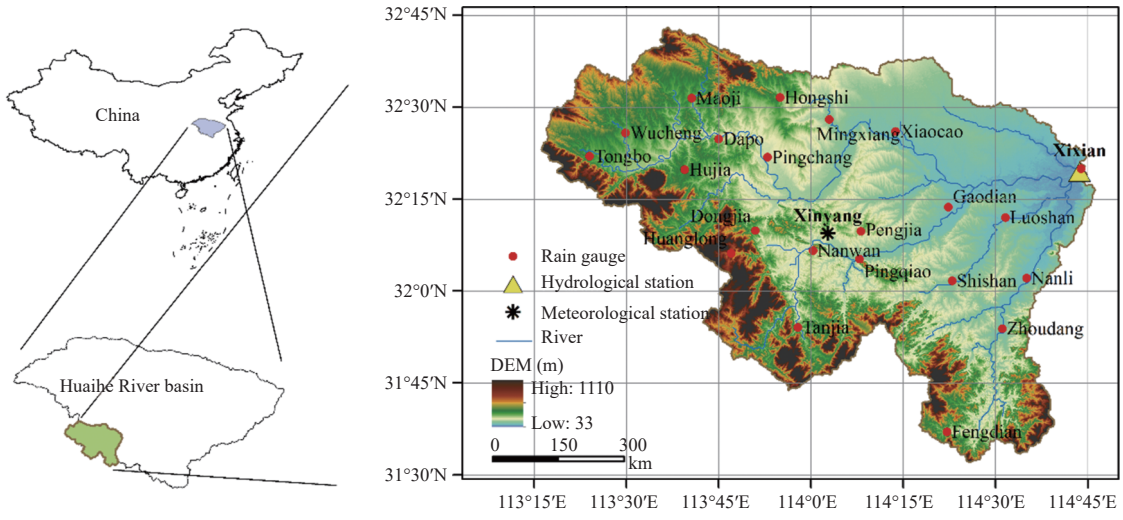

Fig. 1. Locations of the rain gauges, hydrological station, and meteorological station in the study area, and its topography and geographical position.

coefficient of potential evapotranspiration (Kc) predominantly controls the simulated total runoff. The areal mean free water storage capacity (SM) represents the depth of the gravitational water reservoir and largely regulates the magnitude of high flow. The outflow coefficients of the free water storage to interflow and groundwater (KI and KG) determine the flow rate from free water storage and the proportion going to interflow and groundwater flow. The recession constants of surface, interflow, and groundwater runoffs (CS, CI, and CG) regulate the recession rate of each runoff component. For the detailed description of the grid-based XAJ model parameters, please refer to Zhao (1992). In this study, the ratio of impervious area (IM) was calculated by the land cover data, and the rest parameters were automatically calibrated by using the shuffled complex evolution algorithm (SCE-UA; Duan et al., 1994).

3.2 *Statistical indices*

The statistical metrics are separated into two groups in terms of their function (Jiang et al., 2018c). The first group includes the Pearson correlation coefficient (CC), root-mean-square error (RMSE), relative bias (BIAS), and mean error (ME). CC describes the linear correlation in satellite/reanalysis datasets and observed data. BIAS shows systematic bias. RMSE denotes the average error magnitude of the datasets. ME indicates the average differences between the satellite/reanalysis rainfall estimates and rainfall observations. The second group includes the probability of detection (POD) and false alarm ratio (FAR), which present the correspondence between the two fields, as well as the capability for detecting precipitation. POD reflects the probability of rain events correctly detected. FAR indicates false cases when satellite/reanalysis records rainfall while no rain happens. Additionally, to evaluate the capability of simulated streamflow that derived by precipitation products, CC, BIAS, and Nash–Sutcliffe efficiency (NSE) were employed. NSE assesses the goodness of the hydrological model based on the correspondence between simulated runoff and ground observations (Duan et al., 2019; Jiang et al., 2019). Table 2 lists the formulae for metrics mentioned above.

4. Results and discussion

4.1 *Statistical evaluation and comparison of precipitation products*

We evaluate the reanalysis and satellite-based precipitation products against rain gauge precipitation from 2008 to 2015. To ensure a comprehensive comparison, the grid pixels precipitation (22 grids) and basin average precipitation are taken to calculate the statistical metrics, respectively.

Figure 2 shows the density-colored scatterplots of daily precipitation at the grid scale, which compares the

Table 2. Statistical evaluation indices used to evaluate the satellite/reanalysis precipitation products and their capacity for hydrological simulation

Evaluation index	Formula	Comment	Perfect value	Unit
Correlation coefficient (CC)	$\mathrm{CC}=\dfrac{\sum_{i=1}^{n}(G_i-\bar{G})(S_i-\bar{S})}{\sqrt{\sum_{i=1}^{n}(G_i-\bar{G})^2}\sqrt{\sum_{i=1}^{n}(S_i-\bar{S})^2}}$	S_i and G_i are the evaluated and observed values; $\bar{S}$ and $\bar{G}$ are the mean values of S_i and G_i, respectively; n is the number of samples	1	–
Relative bias (BIAS)	$\mathrm{BIAS}=\dfrac{\frac{1}{n}\sum_{i=1}^{n}(S_i-G_i)}{\sum_{i=1}^{n}G_i}\times 100\%$		0	%
Root-mean-square error (RMSE)	$\mathrm{RMSE}=\sqrt{\frac{1}{n}\sum_{i=1}^{n}(S_i-G_i)^2}$		0	mm
Mean error (ME)	$\mathrm{ME}=\frac{1}{n}\sum_{i=1}^{n}(S_i-G_i)$		0	mm
Nash–Sutcliffe efficiency (NSE)	$\mathrm{NSE}=\dfrac{\sum_{i=1}^{n}[Q_{\mathrm{sim}}(i)-Q_{\mathrm{obs}}(i)]^2}{\sum_{i=1}^{n}[Q_{\mathrm{sim}}(i)-\overline{Q}_{\mathrm{obs}}(i)]^2}$		1	–
Probability of detection (POD)	$\mathrm{POD}=\dfrac{t_{\mathrm{H}}}{t_{\mathrm{H}}+t_{\mathrm{M}}}$	t_{H} is the number of observed and detected rainfall events; t_{F} is the number of detected but not observed rainfall events; t_{M} is the number of observed but not detected rainfall events	1	–
False alarm rate (FAR)	$\mathrm{FAR}=\dfrac{t_{\mathrm{F}}}{t_{\mathrm{H}}+t_{\mathrm{F}}}$		0	–

five precipitation products. Except CHIRPS and PERSIANN-CDR, all other three products agree well with the observed data, particularly CMORPH-BLD and CMADS. The results of evaluation metrics at both grid

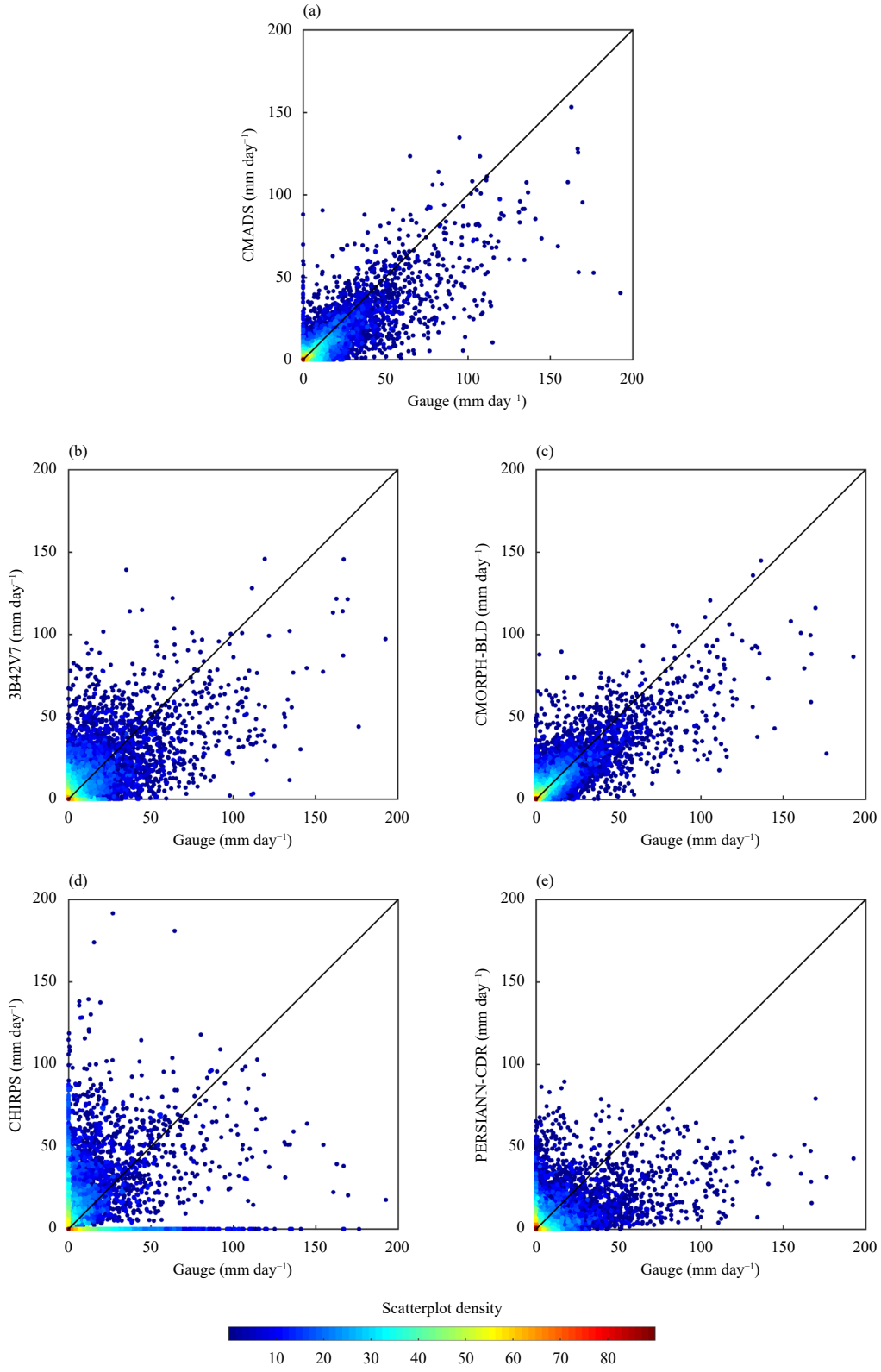

Fig. 2. Density-colored scatterplots of the daily precipitation obtained by (a) CMADS, (b) TMPA 3B42V7, (c) CMORPH-BLD, (d) CHIRPS, and (e) PERSIANN-CDR against the gauge-measured rainfall. The color represents the occurrence frequency, and the solid dark line is the 1:1 line.

and basin scales are summarized in Table 3. The performance of CMORPH-BLD is better than that of the other four products, as it has high CC and low RMSE values (0.85 and 4.91 mm respectively). The performance of CMADS is comparable to that of CMORPH-BLD, for the CC and RMSE values are slightly better, but with a larger BIAS of −20.5%, indicating that it underestimated precipitation. The finding of CMADS underestimation of precipitation is consistent with some previous studies. For instance, Gao et al. (2018) found average bias of −28.7% for CMADS over Xiang River basin and Zhou et al. (2019) conducted average bias of −12.2% for CMADS over Jinhua River basin, which may be caused by the underestimation of the background field CMORPH data. The performance of TMPA 3B42V7 is slightly poorer than that of CMADS, but it outperforms CHIRPS and PERSIANN-CDR. Among these products, PERSIANN-CDR performs the poorest as it exhibits the lowest CC of 0.37 and highest RMSE of 10.9 mm. Based on the systematic error, all products, excluding CMADS, overestimate precipitation. CMORPH-BLD is the best product for detecting rainfall, with the POD reaching 0.95 and low FAR value of 0.3, followed by CMADS, with a POD of 0.91 and FAR of 0.39. As shown in Fig. 3, CMORPH-BLD and CMADS have similar good performance in three metrics: the CC and POD values for these two products are over 0.8 and 0.9 at all station sites respectively, and the FAR values are below 0.5. These results are obviously better than other products, indicating the high accuracy and reliable performances of CMORPH-BLD and CMADS products, which are consistent with some previous research (Sun et al., 2016; Gao et al., 2018). The better performance of CMORPH-BLD and CMADS than TMPA 3B42V7 may be due to the PDF-OI gauge adjustment procedure to correct satellite precipitation, which results in higher quality and more stable performance (Sun et al., 2016). In contrast, TMPA 3B42V7 adopted a simple gauge adjustment algorithm and exhibits relatively poor performance.

At the basin scale, the performance of all five products remarkably improved from their grid-scale performance, as indicated by the increase in the CC values and decrease in the RMSE values. This agrees with previous findings in different regions that increasing the area scale improved the performance of products (Duan et al., 2016; Jiang et al., 2018c; Maggioni and Massari, 2018). As was the case for the grid-scale evaluation, CMORPH-BLD shows outstanding performance with the best CC and RMSE values of 0.95 and 2.58 mm, respectively, then followed by CMADS, and PERSIANN-CDR performs the worst. CMORPH-BLD is the best product for detecting rainfall, with the POD reaching 0.93 and low FAR value of 0.37, followed by CMADS, with a POD of 0.97 and FAR of 0.48. Therefore, both CMORPH-BLD and CMADS could suitably detect rainfall events.

Figure 4 presents the daily precipitation intensities during 2008–2015. The study area predominantly endures light rain (< 1 mm day^{-1}), which accounted for a large number of all rainfall events; this is also shown in Fig. 2. The TMPA 3B42V7 product agrees best with the gauge data for most precipitation classes, particularly for non-rainy and light rainfall (1–10 mm) days. CMORPH-BLD and CMADS generally perform similarly; however, CMORPH-BLD tends to overestimate precipitation ranging from 10 to 50 mm day^{-1}, while CMADS tends to underestimate such rainfall. The underestimation of precipitation over 10 mm day^{-1} by CMADS leads to a significant negative BIAS for the rainfall estimation (Table 3). CHIRPS tends to underestimate precipitation below 25 mm day^{-1}, but overestimate heavy and torrential rainfall (> 25 mm day^{-1}). The result of PERSIANN-CDR is opposite to that of CHIRPS. Excluding CHIRPS, all other four products tend to underestimate torrential rainfall. Notably, although high-intensity precipitation events account for a small percentage of total, they significantly contribute to the total amount of rainfall. As the runoff generation and separation processes within the hydrological models are highly sensitive to the frequency distribution of precipitation, close frequencies to those of the gauge data can ensure accurate hydrological simulation (Tian et al., 2010; Li et al., 2013; Wang et al., 2017).

Taylor diagrams are used to evaluate the performance of the five products at two scales, and simultaneously show the average standard deviation (SD), CC, and RMSE values (Fig. 5). The diagrams provide a concise statistical summary of the indices, in which the products closer to the point representing the gauge observations perform better than the others. CMADS outperforms other

Table 3. Daily evaluation measures of the five precipitation products at the grid and basin scales

SPP	Grid scale						Basin scale					
	CC	ME (mm)	BIAS (%)	RMSE (mm)	POD	FAR	CC	ME (mm)	BIAS (%)	RMSE (mm)	POD	FAR
CMADS	0.86	−0.54	−20.50	4.86	0.91	0.39	0.96	−0.59	−22.72	2.77	0.97	0.48
TMPA 3B42V7	0.70	0.12	5.28	7.02	0.66	0.32	0.80	0.11	4.20	4.83	0.86	0.46
CMORPH-BLD	0.85	0.03	1.57	4.91	0.95	0.30	0.95	0.01	0.47	2.58	0.93	0.37
CHIRPS	0.51	0.23	9.85	8.25	0.77	0.59	0.64	0.38	14.89	7.11	0.68	0.33
PERSIANN-CDR	0.37	0.14	6.26	10.90	0.29	0.42	0.58	0.22	8.50	6.67	0.91	0.49

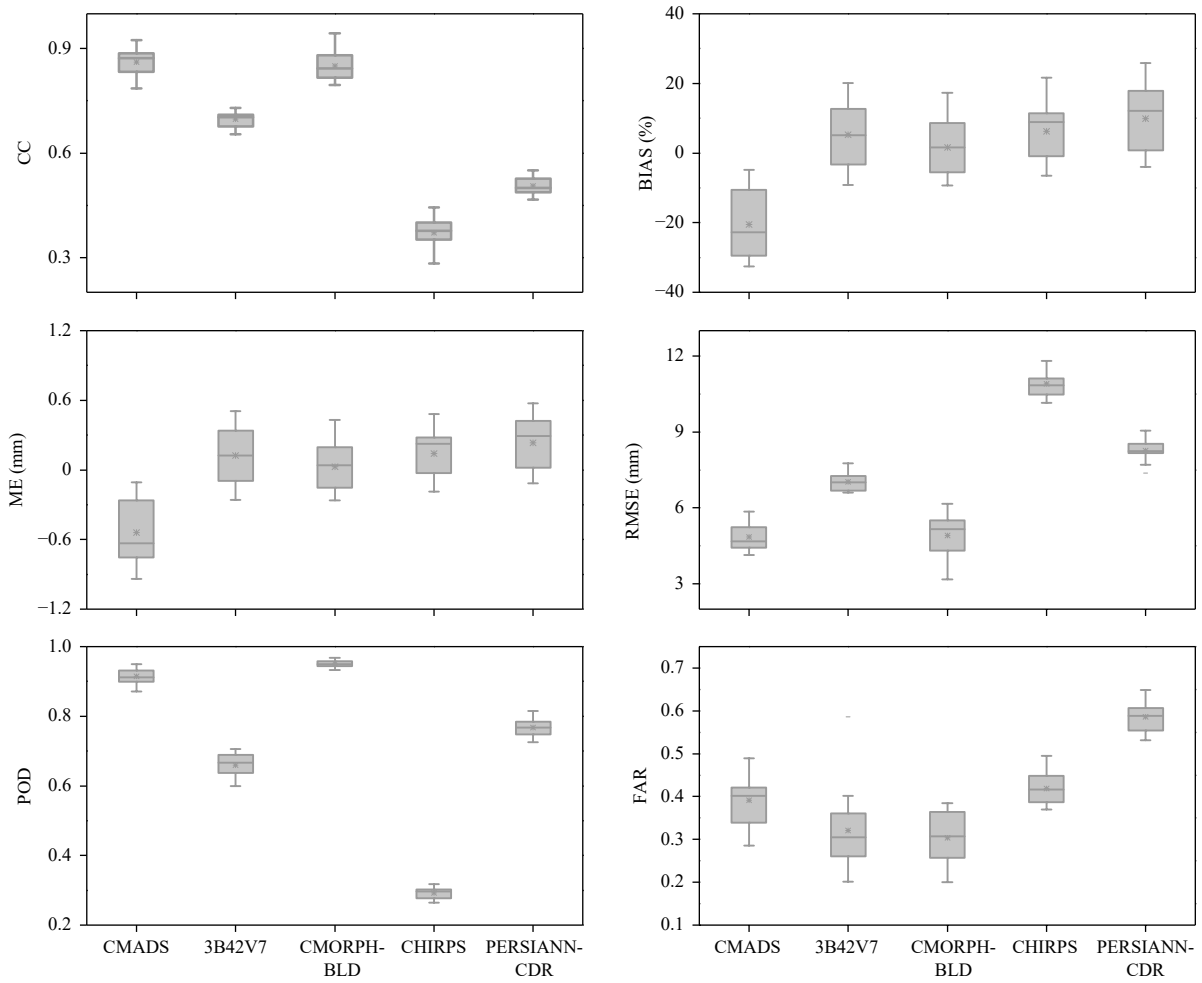

Fig. 3. Box plots of the grid-based metrics of different precipitation products from 2008 to 2015 at daily timescale. The upper and lower edges of the boxes denote the upper and lower quartiles (75% and 25%, respectively), the solid line denotes the median value, and the bars outside the boxes mark the 90th and 10th percentiles, respectively.

products at both the grid and basin scales. The performance of CMORPH-BLD is comparable, though the SD value is slightly higher, and TMPA 3B42V7 exhibits higher SD and RMSE values. The points representing CHIRPS and PERSIANN-CDR are both located far away from the gauge point, indicating relatively poor performance. As expected, all five precipitation products perform better as the scale increased from the grid to the basin, the same as the results of metric evaluation in Table 3.

4.2 *Hydrological utility evaluation*

The suitability of the five precipitation products for hydrological assessments is evaluated by simulating streamflow. The XAJ model is used under two scenarios.

In Scenario I, model parameters are calibrated by using gauge observations as forcing data for calibration period (2008–2012), and the model is verified during the validation period (2013–2015). We then run the model with the five satellite datasets as forcing data by using parameters above.

In Scenario II, the model runs with the same calibration and validation period as Scenario I, except for using the five precipitation data as input data in calibration period, and then individually using the parameters for simulation in validation period.

4.2.1 *Daily streamflow simulations under Scenario I*

Rain gauge data simulations during the whole periods are shown in Fig. 6. The streamflow simulated by using gauge data agrees well with the observations: the NSE values in calibration and validation periods are 0.86 and 0.78, CC values are 0.93 and 0.89, and BIAS values are 1.31% and 11.0%, respectively. Thus, the XAJ model can be reliably used in the Xixian Basin.

The five precipitation products are then used as forcing data for simulating streamflow (Fig. 7 and Table 4).

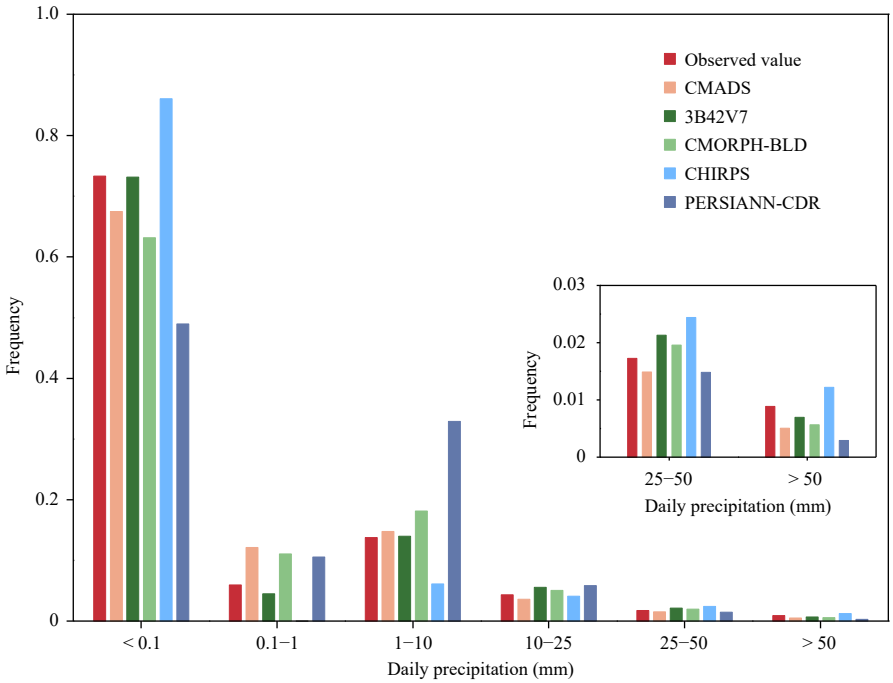

Fig. 4. Occurrence frequencies of different daily precipitation intensities by five precipitation products during 2008–2015.

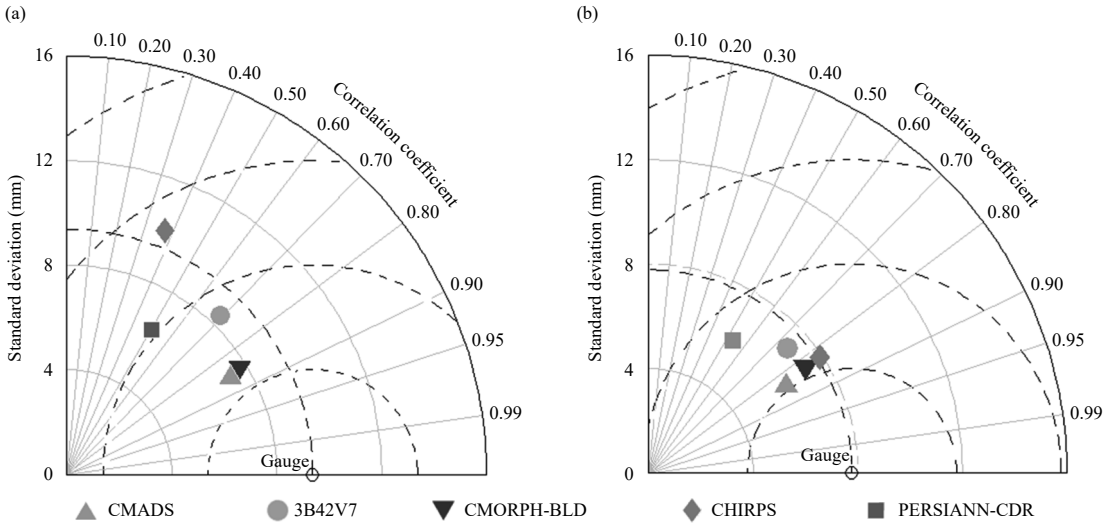

Fig. 5. Taylor diagrams of the five precipitation products against the gauge observations at daily timescale for (a) grid and (b) basin scales.

Generally, CMADS simulates streamflow most accurately throughout both periods, as it exhibited the highest NSE of 0.81 and 0.69, and highest CC of 0.92 and 0.85 for the calibration and validation periods, respectively. However, the simulations significantly underestimate streamflow during the calibration period, with BIAS of −24.8%, which could be due to the underestimation of heavy and torrential rain. The consistent high bias of both the precipitation estimates and streamflow simulation indicates that the error in the rainfall estimates propagates into the hydrological simulations through the hydrological modeling. CMORPH-BLD follows that of CMADS, with slightly lower NSE of 0.76 and 0.53, and CC of 0.88 and 0.73 for the calibration and validation periods, respectively. The results of both TMPA 3B42V7 and CHIRPS are similar, exhibiting similar NSE and CC values. PERSIANN-CDR performs poorly, exhibiting the lowest NSE and CC values and largest negative BIAS. The different biases performance between specific precipitation product and its streamflow simulation may be due to the poor matching of rainfall intensity distributions (Tian et al., 2010; Casse et al., 2015; Maggioni and

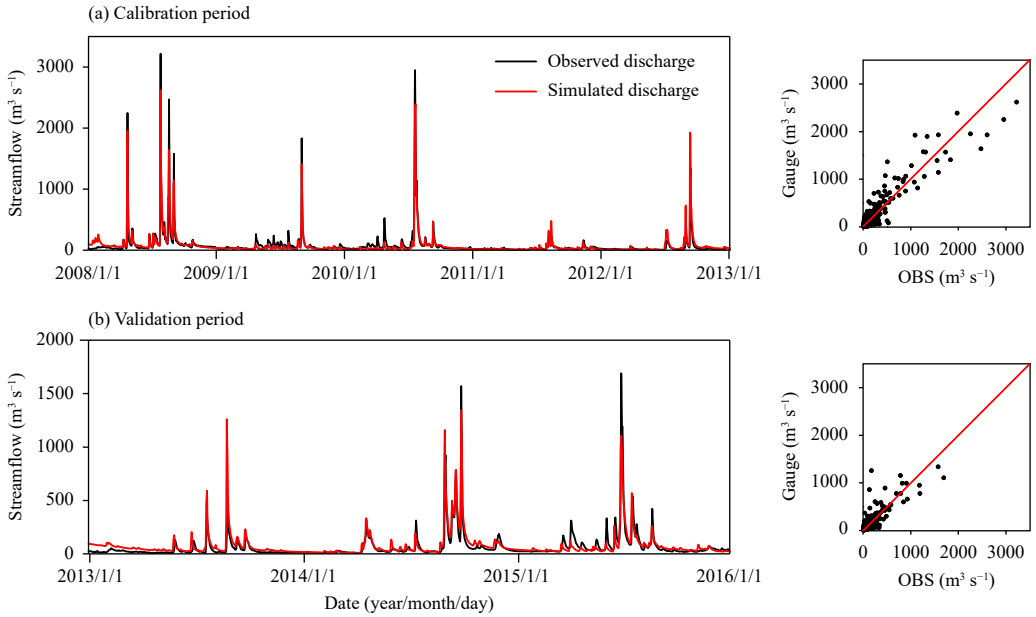

Fig. 6. Comparison of the observed (OBS) and simulated discharges using rain gauge data.

Massari, 2018). For instance, PERSIANN-CDR has significant overestimation (nearly 20%) in light rain (1–10 mm day^{-1}; Fig. 4), and therefore leads to positive bias in rainfall. However, the overestimation in light rain and underestimation in heavy rain of PERSIANN-CDR could affect the streamflow simulation while using parameters calibrated by gauge observations, and might lead to underestimation in streamflow.

4.2.2 *Daily streamflow simulations under Scenario II*

To further evaluate the capability for hydrological simulation, the XAJ model parameters are individually recalibrated by using the five satellite products as input, and the performances are summarized in Fig. 8 and Table 4. All simulations under Scenario II, with higher NSE and CC values, perform better than those under Scenario I, which coincides with previous findings (Jiang et al., 2018c; Maggioni and Massari, 2018). Similar to Scenario I, CMADS outperforms the other products for the entire period, with the highest NSE and CC values: for calibration period they are 0.85 and 0.92, and for validation period they are 0.75 and 0.85, respectively. Unlike the high BIAS under Scenario I, the BIAS exhibits reasonable values under Scenario II, with values of −2.71% in calibration period and 5.10% in validation period, respectively, indicating that the recalibration of model parameters compensates for the rainfall underestimation by the products, thus improving the hydrological performance of the model. The CMADS-calibrated model captures most of the peak flows, as shown in the scatterplots in Fig. 8. However, the simulations tend to underestimate discharge when capturing high peak flows, which is partly due to the uncertainty in the detection of heavy and torrential rainfall events by CMADS as shown in Fig. 4.

4.3 *Discussion*

4.3.1 *Effects of model recalibration on streamflow simulation*

The effects of recalibration on model parameters and streamflow simulation when using specific precipitation data as input are further analyzed. Table 5 shows the parameters of the grid-based XAJ model calibrated with gauge observation and each specific precipitation data as input for the calibration period 2008–2012. The Kc is a sensitive parameter that can predominantly control the simulated total runoff. When the Kc value is increased, the calculated evapotranspiration also increases; conversely, the evapotranspiration decreases. For the significant negative bias of the streamflow simulations for the CMADS, CMORPH-BLD, and PERSIANN-CDR products, the recalibration reduced the Kc values from 1.49 to 0.96, 1.33, and 1.25 to achieve a good simulation of the streamflow (see Table 4), respectively. The SM predominantly regulates the high flow magnitude, and reducing SM tends to partition a larger proportion of surface runoff from the total runoff and hence produces high flood peaks (Zhao, 1992). Under Scenario II, the model recalibration alleviates the magnitudes of high-flow underestimation (Figs. 8a, b, e) via decreasing SM from 46.25 to 32.2 mm for CMADS, 22.38 mm for 3B42V7, and 43.32 mm for PERSIANN-CDR. The KI and KG determine the flow rate from free water storage and the pro-

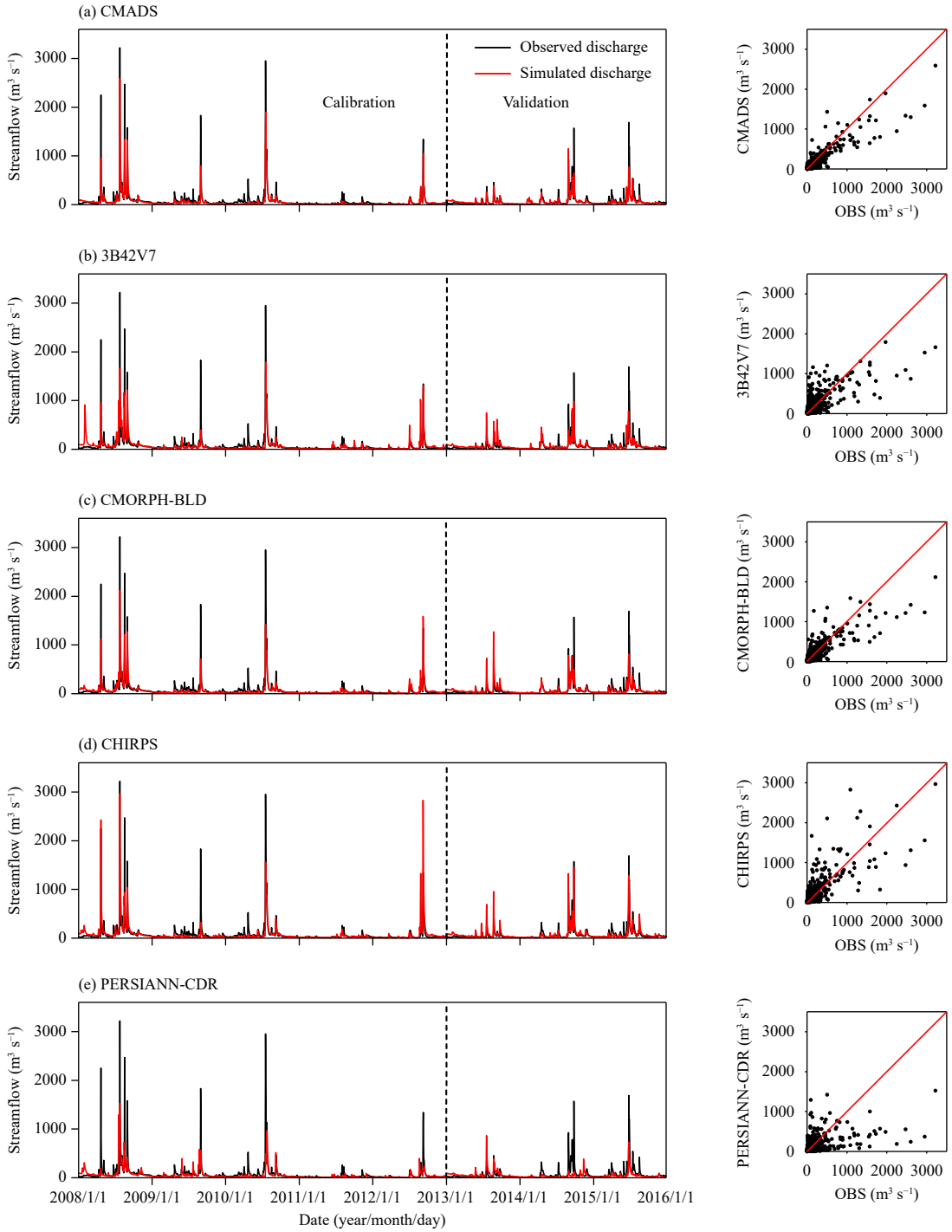

Fig. 7. Comparison of the observed and simulated discharges by (a) CMADS, (b) TMPA 3B42V7, (c) CMORPH-BLD, (d) CHIRPS, and (e) PERSIANN-CDR at the Xixian Station under Scenario I.

portion going to interflow and groundwater flow, and a larger KI can produce higher flood peaks. The model recalibration alleviates the magnitudes of high-flow underestimation (Fig. 8) via increasing KI from 0.36 to 0.37 for CMADS, 0.41 for CMORPH-BLD, and 0.44 for PERSIANN-CDR. Moreover, reducing the recession constants of surface, interflow, and groundwater runoffs (CS, CI, and CG) may lead to a faster recession rate for each runoff component and consequently augment high flows to a certain extent. Table 5 shows that the CS value of CMORPH-BLD and CI values of five precipitation products had reduced, thereby partially compensating for the high-flow underestimation. By recalibration, the model sensitive parameters are mostly changed into the

Table 4. Evaluation indices of the hydrological simulation results of the five precipitation products

Calibration scenario	Precipitation product	Calibration period (CP)			Validation period (VP)		
		CC	NSE	BIAS (%)	CC	NSE	BIAS (%)
Scenario I	Gauge	0.93	0.86	1.31	0.89	0.78	11.00
	CMADS	0.92	0.81	−24.80	0.85	0.69	−9.18
	TMPA 3B42V7	0.78	0.61	−3.48	0.72	0.51	8.40
	CMORPH-BLD	0.88	0.76	−14.00	0.73	0.53	9.60
	CHIRPS	0.79	0.58	−2.65	0.82	0.62	16.20
	PERSIANN-CDR	0.58	0.33	−25.10	0.47	0.22	−22.90
Scenario II	CMADS	0.92	0.85	−2.71	0.85	0.75	5.10
	TMPA 3B42V7	0.79	0.63	0.36	0.74	0.55	9.40
	CMORPH-BLD	0.89	0.78	−2.20	0.76	0.70	9.87
	CHIRPS	0.83	0.65	4.32	0.81	0.63	9.64
	PERSIANN-CDR	0.64	0.41	−5.77	0.57	0.32	−2.93

direction that makes the simulation better. However, it should be noted that for the complexity and uncertainty of the model parameters, not all the recalibrated parameters of specific precipitation product changed consistently, which could be attributed to the equifinality for different parameters (Beven and Freer, 2001).

Model recalibration has also been proved to be a viable strategy for improving satellite and reanalysis precipitation-forced hydrological model performances in some other basins of different size and climatology in Ethiopia, China, and Myanmar (Bitew and Gebremichael, 2011; Jiang et al., 2012; Maggioni and Massari, 2018; Yuan et al., 2019). The reason can be attributed to the different precision characteristics of the satellite and reanalysis precipitation with respect to the gauge measurements. The recalibrated parameter settings can compensate for the inaccurate satellite and reanalysis precipitation errors to some extent, thereby improving streamflow simulations with respect to the gauge observations calibration option (see Tables 4 and 5). However, it is worth noting that the recalibration cannot completely compensate for the errors from inaccurate precipitation forcing input. After the parameter recalibration, the most inaccurate precipitation (i.e., the PERSIANN-CDR precipitation product in this study) still had the largest streamflow simulation error in terms of CC and NSE values (see Table 4). This could be related to the threshold gain function in error transfer of the hydrological model and parameter recalibration; that is, if the precipitation input error is higher than a certain threshold, the streamflow output error will be hard to eliminate, and if the precipitation input error is lower than a certain threshold, the runoff output error will not increase much, or even decline (Yong et al., 2010; Jiang et al., 2012; Mei et al., 2016).

4.3.2 *Comparison with the findings of other CMADS studies*

The results of recent studies evaluating the applicability of the CMADS precipitation product to simulate streamflow over the Chinese mainland are summarized in Table 6. For precipitation estimation, based on the CC values, the accuracy of the CMADS precipitation product in humid regions (such as the Xiang and Jinhua River basins, and Huaihe River source basin) is higher than that in semiarid regions (such as the Yellow River source basin), indicating that the CMADS could estimate precipitation in the humid regions of Chinese mainland well. In terms of the BIAS values, the CMADS precipitation product tends to underestimate precipitation in humid regions, but overestimate precipitation in semiarid regions. The bias in the background data and assimilation algorithm, unevenly distributed rain gauge stations, and the complex topography of some regions may have attributed to the high bias of the CMADS precipitation estimates. For streamflow simulation, most studies (except for Jinhua River and Xihe River basins) reported good performance with satisfactory NSE and BIAS values owing to parameter recalibration, which compensated for the bias in the rainfall results. Overall, these results demonstrate the outstanding hydrological performance of the CMADS precipitation product, and suggest that CMADS is suitable for various regions in China, particularly humid regions.

4.3.3 *Performance of CMADS precipitation estimates for the Chinese mainland*

Owing to the remarkable performance of CMADS for estimating precipitation and simulating streamflow in recent studies, its applicability in different climates and elevation bands should be assessed. We further evaluate its performance for the Chinese mainland by calculating the CC, BIAS, POD, and FAR against data from 824 rain gauges collected during 2008–2015. Figure 9 shows the rain gauge distribution which is relatively evenly spaced throughout the Chinese mainland.

Figure 9 plots the spatial distributions of the metrics for the CMADS estimates over Chinese mainland. The distributions of CC and POD are identical, and declined from southeast to northwest. This trend is also similar to

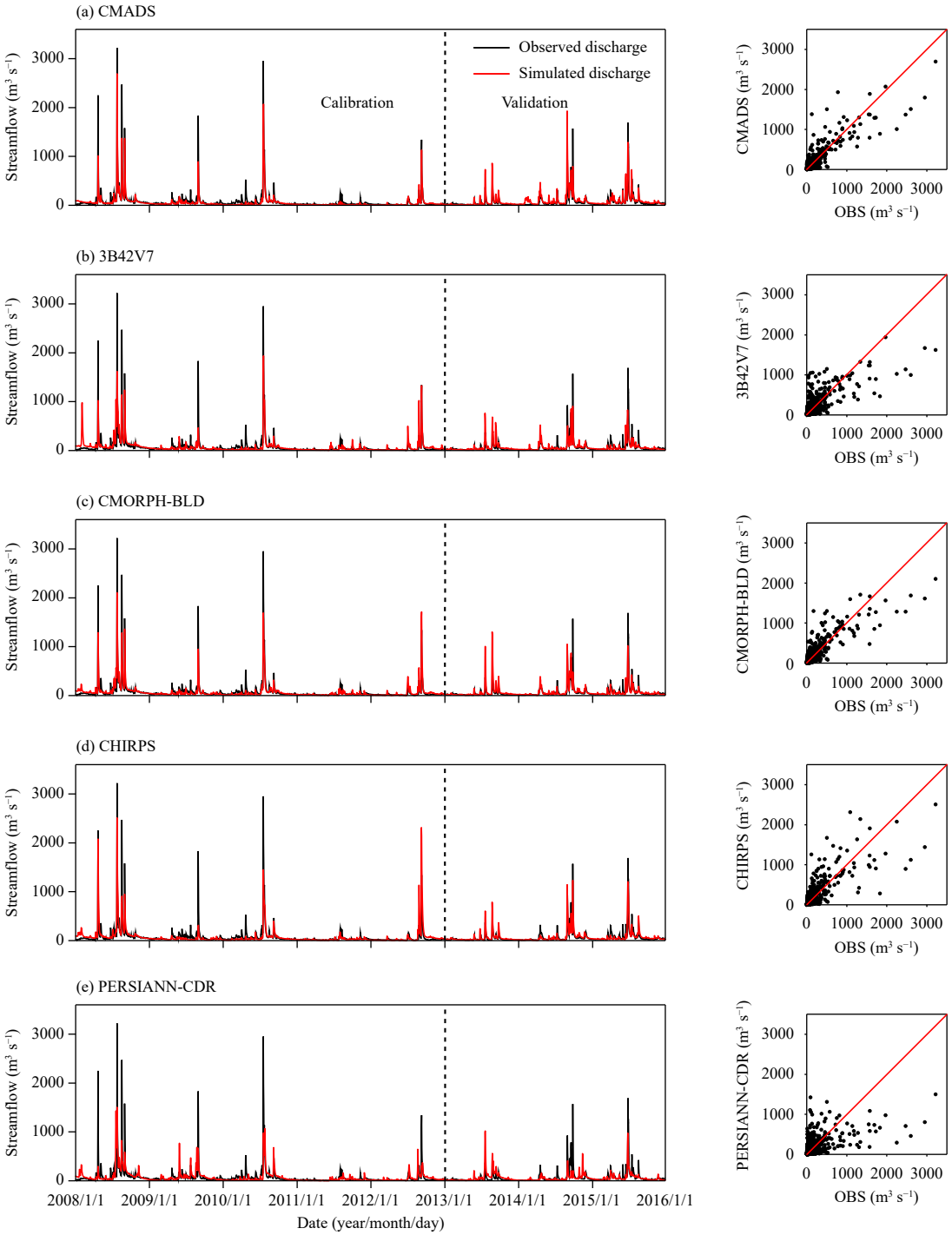

Fig. 8. As in Fig. 7, but for Scenario II.

the precipitation intensity distribution over the Chinese mainland, i.e., the decline of CC and POD values coincides with the declination of the precipitation intensity. The CC and POD of CMADS are generally high in eastern and southwestern China, where heavy rainfall events frequently occur. However, the CC and POD values are lower in northwestern China. The complexity of the climate and topography in such areas challenges the accuracy of satellite precipitation estimates, particularly in mountainous regions (i.e., the Tibetan Plateau), which resulted in the low CC and POD values. Moreover, interpolated rainfall errors are more likely to occur in areas with a sparse gauge network, increasing the uncertainty of precipitation estimates. Therefore, apart from the satellite retrieval algorithm, the low accuracy of precipitation estimates over these areas could also be due to the

Table 5. Parameters commonly used in the XAJ model, their prior ranges, and values calibrated by gauge observation and specific precipitation products

Parameter	Prior range	Default value	Value of calibrated model parameter					
			Gauge	CMADS	3B42V7	CMORPH-BLD	CHIRPS	PERSIANN-CDR
Kc	0.8–1.5	1.2	1.49	0.96	1.49	1.33	1.49	1.25
WUM	10–40	20.0	30.00	28.13	30.00	29.91	22.04	23.36
WLM	50–90	60.0	65.62	60.43	59.21	61.81	63.27	67.82
WDM	10–70	40.0	35.26	37.89	49.99	30.00	40.83	49.79
B	0.1–0.5	0.3	0.18	0.11	0.27	0.15	0.14	0.11
IM	0.03	0.03	0.03	0.03	0.03	0.03	0.03	0.03
C	0.1–0.3	0.2	0.20	0.15	0.20	0.20	0.15	0.15
EX	1.0–1.5	1.2	1.27	1.45	1.43	1.47	1.00	1.03
SM	10–60	20.0	46.25	32.20	22.38	46.79	50.00	43.32
KI	KI + KG = 0.7	0.4	0.36	0.37	0.33	0.41	0.25	0.44
KG	0.1–0.5	0.3	0.34	0.33	0.37	0.29	0.45	0.26
CS	0.1–0.5	0.2	0.35	0.44	0.44	0.31	0.42	0.50
CI	0.1–0.9	0.5	0.82	0.81	0.71	0.68	0.64	0.57
CG	0.9–0.999	0.9	0.99	0.99	0.99	0.99	0.99	0.98
KE	20–24	24.0	21.41	20.00	21.58	23.59	23.64	20.00
XE	0.1–0.5	0.5	0.50	0.50	0.50	0.50	0.50	0.50

Note: The parameters that are in bold and underlined are model sensitive parameters. For the meanings of WUM, WLM, WDM, *B*, *C*, EX, KE, and XE, please refer to Zhao (1992) and Yuan et al. (2019).

Table 6. Summary of previous hydrological studies on the CMADS precipitation product

Reference	Evaluation period	Study area	Area (km^2)	Latitude	Model	Calibration	Precipitation		Streamflow	
							CC	BIAS (%)	NSE	BIAS (%)
This study	2008–2015	Huaihe River source basin	10,191	31°–33°N	XAJ	CMADS data	0.96	−22.72	0.85 in CP, 0.75 in VP	−2.71 in CP, 5.1 in VP
Gao et al. (2018)	2008–2013	Xiang River basin	82,375	24°–28°N	SWAT	CMADS data	0.70	−28.67	0.83 in CP, 0.70 in VP	−12.06 in CP, 2.2 in VP
Guo et al. (2018)	2009–2016	Lijiang River basin	2591	25°N	IHACRES	CMADS data	–	–	0.69 in CP, 0.70 in VP	−21 in CP, −7 in VP
Zhou et al. (2019)	2008–2013	Jinhua River basin	6782	28°–29°N	DHSVM	Gauge observations	0.77	−12.15	0.56 in CP, 0.61 in VP	−44.42 in CP, −33.29 in VP
Liu et al. (2018)	2009–2013	Yellow River source basin	123,700	32°–36°N	SWAT	CMADS data	0.46	8.00	0.63 in CP, 0.59 in VP	–
Li et al. (2019)	2009–2013	Jing and Bortala River basins	11,300	44°–45°N	SWAT	CMADS data	–	–	0.80 in CP, 0.85 in VP	–
Wang et al. (2020)	2008–2015	Xihe River basin	1267	34°–35°N	SWAT	Gauge observations	0.93	−10.9	−0.43	95.22

sparse gauge network. The FAR demonstrates similar spatial distribution of precipitation precision with CC and POD. The high POD and low FAR values in southeastern China indicate that CMADS could detect and capture rainfall events in this region. Similar to our study area, CMADS underestimates the precipitation over most regions with relatively high bias, as shown in Fig. 9b. CMADS tends to underestimate precipitation across most regions of China, and overestimate precipitation in areas with limited rainfall and sparsely distributed rain gauge stations. Owing to the significant underestimation of rainfall in most regions of China, researchers should proceed with caution when applying CMADS precipitation product to simulate and predict hydrological extremes.

5. Conclusions

In this study, the performance of one recently released reanalysis precipitation dataset (CMADS) and four bias-adjusted satellite precipitation datasets (TMPA 3B42V7, CMORPH-BLD, CHIRPS, and PERSIANN-CDR) was evaluated and compared against rain gauge observations at the grid and basin scales. The performance of these products in driving the XAJ model for streamflow simulation was also assessed. The major conclusions are summarized as follows.

For statistical assessment, the CMADS reanalysis and CMORPH-BLD satellite precipitation datasets both perform similarly, with high CC and low RMSE values. Notably, CMADS generally underestimates precipitation while the other products present reasonable bias. Generally, CMADS and CMORPH-BLD both perform the best, followed by TMPA 3B42V7, while CHIRPS and PERSIANN-CDR perform poorly. CMORPH-BLD performs the best in capturing and detecting rainfall events. While CMADS tends to underestimate heavy and torren-

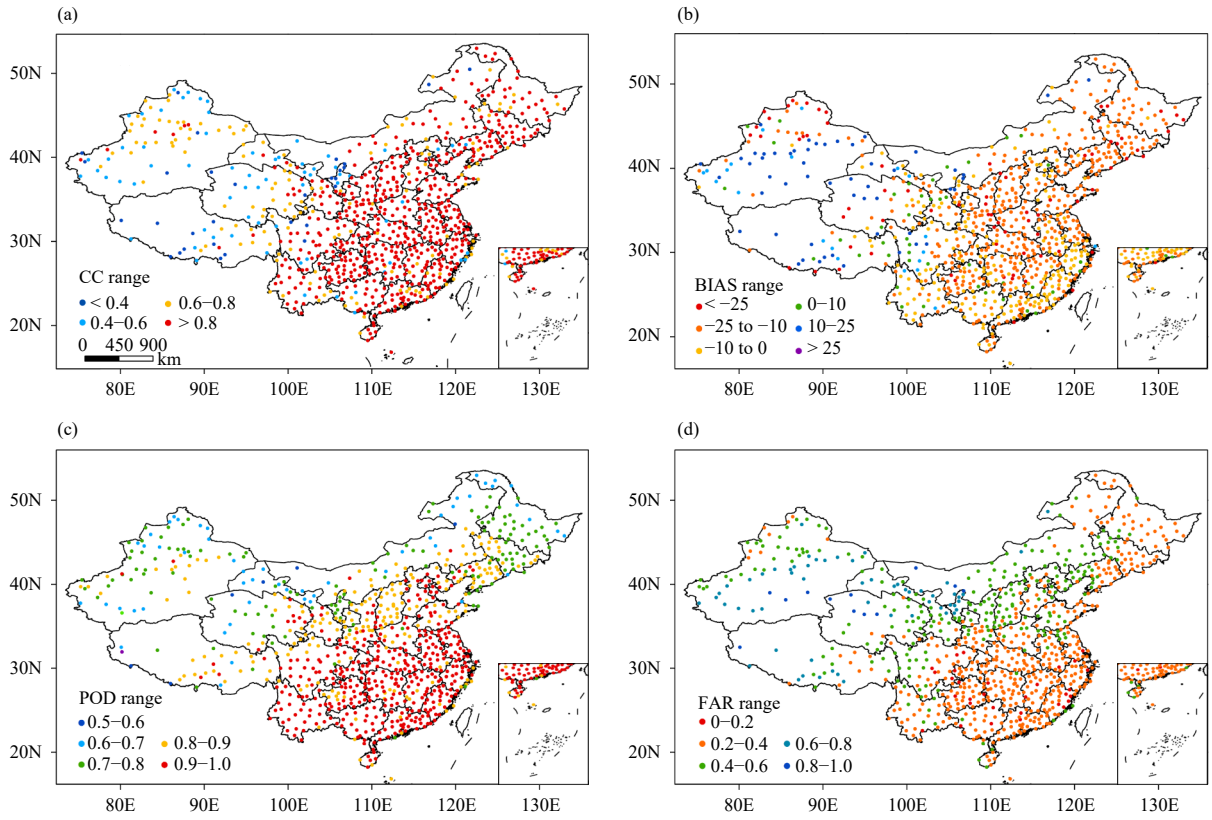

Fig. 9. Spatial distributions of the (a) CC, (b) BIAS, (c) POD, and (d) FAR of CMADS against the rainfall observed by gauges throughout the Chinese mainland during 2008–2015.

tial precipitation, and the underestimation may have contributed to the significant bias in the evaluation of precipitation.

The results of the streamflow simulations under Scenario I show that CMADS outperforms CMORPH-BLD. Under Scenario II, the simulation performances of all five precipitation products are significantly better than those under Scenario I. Despite the high negative bias in the statistical evaluation of CMADS precipitation, the bias of streamflow simulation under Scenario II is reasonable, demonstrating that the CMADS precipitation product is applicable to hydrological evaluation and simulation.

The spatial distribution of the evaluation metrics of CMADS over Chinese mainland is similar to that of precipitation intensity, which exhibits high accuracy in eastern China and declines from southeast to northwest. Despite the rain gauge density, performance of the metrics is also affected by the climate and elevation conditions, resulting in the poor performance in northwestern China.

Overall, the CMADS reanalysis precipitation dataset could provide reasonably good rainfall estimation and can drive hydrological model to generate good runoff simulation in the Xixian Basin. CMORPH-BLD and CMADS products show similar performance and are comparable with each other, as the CMADS precipitation product uses CMORPH as a background field. However, owing to the high negative BIAS values of CMADS precipitation data, the CMADS research community should further improve the calibration algorithms and enhance the quality of the precipitation product for eastern Asia. In addition, this study only evaluated CMADS against a limited number of SPPs. In the future, we should further strengthen the scientific evaluation and practical application of CMADS, such as comparing CMADS with the latest Integrated Multi-satellite Retrievals for GPM Version 6 products (Huffman et al., 2019).

Acknowledgments. The CMADS, TMPA 3B42V7, CMORPH-BLD, CHIRPS, and PERSIANN-CDR were freely obtained from their corresponding data centers. The authors are grateful to the Editor and two anonymous reviewers for providing insightful comments that have significantly improved the quality of this paper.

REFERENCES

Bartier, P. M., and C. P. Keller, 1996: Multivariate interpolation to incorporate thematic surface data using inverse distance

weighting (IDW). *Comput. Geosci.*, **22**, 795–799, doi: 10.1016/0098-3004(96)00021-0.

Beven, K., and J. Freer, 2001: Equifinality, data assimilation, and uncertainty estimation in mechanistic modelling of complex environmental systems using the GLUE methodology. *J. Hydrol.*, **249**, 11–29, doi: 10.1016/S0022-1694(01)00421-8.

Bitew, M. M., and M. Gebremichael, 2011: Evaluation of satellite rainfall products through hydrologic simulation in a fully distributed hydrologic model. *Water Resour. Res.*, **47**, W06526, doi: 10.1029/2010WR009917.

Casse, C., M. Gosset, C. Peugeot, et al., 2015: Potential of satellite rainfall products to predict Niger River flood events in Niamey. *Atmos. Res.*, **163**, 162–176, doi: 10.1016/j.atmosres.2015.01.010.

Chen, T., L. L. Ren, F. Yuan, et al., 2019: Merging ground and satellite-based precipitation data sets for improved hydrological simulations in the Xijiang River basin of China. *Stoch. Environ. Res. Risk Assess.*, **33**, 1893–1905, doi: 10.1007/s00477-019-01731-w.

Dee, D. P., S. M. Uppala, A. J. Simmons, et al., 2011: The ERA-Interim reanalysis: Configuration and performance of the data assimilation system. *Quart. J. Roy. Meteor. Soc.*, **137**, 553–597, doi: 10.1002/qj.828.

Duan, Q. Y., S. Sorooshian, and V. K. Gupta, 1994: Optimal use of the SCE-UA global optimization method for calibrating watershed models. *J. Hydrol.*, **158**, 265–284, doi: 10.1016/0022-1694(94)90057-4.

Duan, Z., J. Z. Liu, Y. Tuo, et al., 2016: Evaluation of eight high spatial resolution gridded precipitation products in Adige Basin (Italy) at multiple temporal and spatial scales. *Sci. Total Environ.*, **573**, 1536–1553, doi: 10.1016/j.scitotenv.2016.08.213.

Duan, Z., Y. Tuo, J. Z. Liu, et al., 2019: Hydrological evaluation of open-access precipitation and air temperature datasets using SWAT in a poorly gauged basin in Ethiopia. *J. Hydrol.*, **569**, 612–626, doi: 10.1016/j.jhydrol.2018.12.026.

Friedl, M. A., D. K. McIver, J. C. F. Hodges, et al., 2002: Global land cover mapping from MODIS: Algorithms and early results. *Remote Sens. Environ.*, **83**, 287–302, doi: 10.1016/S0034-4257(02)00078-0.

Funk, C., P. Peterson, M. Landsfeld, et al., 2015: The climate hazards infrared precipitation with stations—a new environmental record for monitoring extremes. *Sci. Data*, **2**, 150066, doi: 10.1038/sdata.2015.66.

Gao, X. C., Q. Zhu, Z. Y. Yang, et al., 2018: Evaluation and hydrological application of CMADS against TRMM 3B42V7, PERSIANN-CDR, NCEP-CFSR, and gauge-based datasets in Xiang River basin of China. *Water*, **10**, 1225, doi: 10.3390/w10091225.

Gao, Z., D. Long, G. Q. Tang, et al., 2017: Assessing the potential of satellite-based precipitation estimates for flood frequency analysis in ungauged or poorly gauged tributaries of China's Yangtze River basin. *J. Hydrol.*, **550**, 478–496, doi: 10.1016/j.jhydrol.2017.05.025.

Gebregiorgis, A. S., P.-E. Kirstetter, Y. E. Hong, et al., 2018: To what extent is the day 1 GPM IMERG satellite precipitation estimate improved as compared to TRMM TMPA-RT? *J. Geophys. Res. Atmos.*, **123**, 1694–1707, doi: 10.1002/2017JD027606.

Gelaro, R., W. McCarty, M. J. Suárez, et al., 2017: The Modern-Era Retrospective Analysis for Research and Applications, version 2 (MERRA-2). *J. Climate*, **30**, 5419–5454, doi: 10.1175/JCLI-D-16-0758.1.

Golian, S., S. Moazami, P.-E. Kirstetter, et al., 2015: Evaluating the performance of merged multi-satellite precipitation products over a complex terrain. *Water Resour. Manag.*, **29**, 4885–4901, doi: 10.1007/s11269-015-1096-6.

Golian, S., M. Javadian, and A. Behrangi, 2019: On the use of satellite, gauge, and reanalysis precipitation products for drought studies. *Environ. Res. Lett.*, **14**, 075005, doi: 10.1088/1748-9326/ab2203.

Guo, B. B., J. Zhang, T. B. Xu, et al., 2018: Applicability assessment and uncertainty analysis of multi-precipitation datasets for the simulation of hydrologic models. *Water*, **10**, 1611, doi: 10.3390/w10111611.

Guo, H., A. M. Bao, T. Liu, et al., 2016: Evaluation of PERSIANN-CDR for meteorological drought monitoring over China. *Remote Sens.*, **8**, 379, doi: 10.3390/rs8050379.

Hou, A. Y., R. K. Kakar, S. Neeck, et al., 2014: The Global Precipitation Measurement mission. *Bull. Amer. Meteor. Soc.*, **95**, 701–722, doi: 10.1175/BAMS-D-13-00164.1.

Huffman, G. J., D. T. Bolvin, E. J. Nelkin, et al., 2007: The TRMM Multisatellite Precipitation Analysis (TMPA): Quasi-global, multiyear, combined-sensor precipitation estimates at fine scales. *J. Hydrometeor.*, **8**, 38–55, doi: 10.1175/JHM560.1.

Huffman, G. J., D. T. Bolvin, D. Braithwaite, et al., 2019: NASA Global Precipitation Measurement (GPM) Integrated Multi-SatellitE Retrievals for GPM (IMERG). Algorithm Theoretical Basis Document (ATBD) Version 06, NASA, Washington, 34 pp.

Jiang, S. H., L. L. Ren, Y. Hong, et al., 2012: Comprehensive evaluation of multi-satellite precipitation products with a dense rain gauge network and optimally merging their simulated hydrological flows using the Bayesian model averaging method. *J. Hydrol.*, **452–453**, 213–225, doi: 10.1016/j.jhydrol.2012.05.055.

Jiang, S. H., L. L. Ren, Y. Hong, et al., 2014: Improvement of multi-satellite real-time precipitation products for ensemble streamflow simulation in a middle latitude basin in South China. *Water Resour. Manag.*, **28**, 2259–2278, doi: 10.1007/s11269-014-0612-4.

Jiang, S. H., L. L. Ren, C.-Y. Xu, et al., 2018a: Quantifying multi-source uncertainties in multi-model predictions using the Bayesian model averaging scheme. *Hydrol. Res.*, **49**, 954–970, doi: 10.2166/nh.2017.272.

Jiang, S. H., S. Y. Liu, L. L. Ren, et al., 2018b: Hydrologic evaluation of six high resolution satellite precipitation products in capturing extreme precipitation and streamflow over a medium-sized basin in China. *Water*, **10**, 25, doi: 10.3390/w10010025.

Jiang, S. H., L. L. Ren, C.-Y. Xu, et al., 2018c: Statistical and hydrological evaluation of the latest Integrated Multi-SatellitE Retrievals for GPM (IMERG) over a midlatitude humid basin in South China. *Atmos. Res.*, **214**, 418–429, doi: 10.1016/j.atmosres.2018.08.021.

Jiang, S. H., M. H. Wang, L. L. Ren, et al., 2019: A framework for quantifying the impacts of climate change and human activit-

ies on hydrological drought in a semiarid basin of northern China. *Hydrol. Process.*, **33**, 1075–1088, doi: 10.1002/hyp.13386.

Joyce, R. J., J. E. Janowiak, P. A. Arkin, et al., 2004: CMORPH: A method that produces global precipitation estimates from passive microwave and infrared data at high spatial and temporal resolution. *J. Hydrometeor.*, **5**, 487–503, doi: 10.1175/1525-7541(2004)005<0487:CAMTPG>2.0.CO;2.

Lai, C. G., R. D. Zhong, Z. L. Wang, et al., 2019: Monitoring hydrological drought using long-term satellite-based precipitation data. *Sci. Total Environ.*, **649**, 1198–1208, doi: 10.1016/j.scitotenv.2018.08.245.

Li, Y., Y. J. Wang, J. H. Zheng, et al., 2019: Investigating spatial and temporal variation of hydrological processes in western China driven by CMADS. *Water*, **11**, 435, doi: 10.3390/w11030435.

Li, Z., D. W. Yang, and Y. Hong, 2013: Multi-scale evaluation of high-resolution multi-sensor blended global precipitation products over the Yangtze River. *J. Hydrol.*, **500**, 157–169, doi: 10.1016/j.jhydrol.2013.07.023.

Liu, J., D. H. Shanguan, S. Y. Liu, et al., 2018: Evaluation and hydrological simulation of CMADS and CFSR reanalysis datasets in the Qinghai–Tibet Plateau. *Water*, **10**, 513, doi: 10.3390/w10040513.

Maggioni, V., and C. Massari, 2018: On the performance of satellite precipitation products in riverine flood modeling: A review. *J. Hydrol.*, **558**, 214–224, doi: 10.1016/j.jhydrol.2018.01.039.

Maggioni, V., P. C. Meyers, and M. D. Robinson, 2016: A review of merged high-resolution satellite precipitation product accuracy during the Tropical Rainfall Measuring Mission (TRMM) era. *J. Hydrometeor.*, **17**, 1101–1117, doi: 10.1175/JHM-D-15-0190.1.

Mei, Y. W., E. I. Nikolopoulos, E. N. Anagnostou, et al., 2016: Evaluating satellite precipitation error propagation in runoff simulations of mountainous basins. *J. Hydrometeor.*, **17**, 1407–1423, doi: 10.1175/JHM-D-15-0081.1.

Meng, X. Y., and H. Wang, 2017: Significance of the China Meteorological Assimilation Driving Datasets for the SWAT model (CMADS) of East Asia. *Water*, **9**, 765, doi: 10.3390/w9100765.

Meng, X. Y., H. Wang, C. X. Shi, et al., 2018: Establishment and evaluation of the China Meteorological Assimilation Driving Datasets for the SWAT model (CMADS). *Water*, **10**, 1555, doi: 10.3390/w10111555.

Saha, S., S. Moorthi, H.-L. Pan, et al., 2010: The NCEP Climate Forecast System Reanalysis. *Bull. Amer. Meteor. Soc.*, **91**, 1015–1058, doi: 10.1175/2010BAMS3001.1.

Sahoo, A. K., J. Sheffield, M. Pan, et al., 2015: Evaluation of the Tropical Rainfall Measuring Mission Multi-Satellite Precipitation Analysis (TMPA) for assessment of large-scale meteorological drought. *Remote Sens. Environ.*, **159**, 181–193, doi: 10.1016/j.rse.2014.11.032.

Seyyedi, H., E. N. Anagnostou, E. Beighley, et al., 2015: Hydrologic evaluation of satellite and reanalysis precipitation datasets over a mid-latitude basin. *Atmos. Res.*, **164–165**, 37–48, doi: 10.1016/j.atmosres.2015.03.019.

Shi, P., C. Chen, R. Srinivasan, et al., 2011: Evaluating the SWAT model for hydrological modeling in the Xixian Watershed and a comparison with the XAJ model. *Water Resour. Manag.*, **25**, 2595–2612, doi: 10.1007/s11269-011-9828-8.

Skofronick-Jackson, G., W. A. Petersen, W. Berg, et al., 2017: The Global Precipitation Measurement (GPM) mission for science and society. *Bull. Amer. Meteor. Soc.*, **98**, 1679–1695, doi: 10.1175/BAMS-D-15-00306.1.

Sorooshian, S., K.-L. Hsu, X. G. Gao, et al., 2000: Evaluation of PERSIANN system satellite-based estimates of tropical rainfall. *Bull. Amer. Meteor. Soc.*, **81**, 2035–2046, doi: 10.1175/1520-0477(2000)081<2035:EOPSSE>2.3.CO;2.

Su, J. B., H. S. Lü, J. Q. Wang, et al., 2017: Evaluating the applicability of four latest satellite–gauge combined precipitation estimates for extreme precipitation and streamflow predictions over the upper Yellow River basins in China. *Remote Sens.*, **9**, 1176, doi: 10.3390/rs9111176.

Sulugodu, B., and P. C. Deka, 2019: Evaluating the performance of CHIRPS satellite rainfall data for streamflow forecasting. *Water Resour. Manag.*, **33**, 3913–3927, doi: 10.1007/s11269-019-02340-6.

Sun, Q. H., C. Y. Miao, Q. Y. Duan, et al., 2018: A review of global precipitation data sets: Data sources, estimation, and intercomparisons. *Rev. Geophys.*, **56**, 79–107, doi: 10.1002/2017RG000574.

Sun, R. C., H. L. Yuan, X. L. Liu, et al., 2016: Evaluation of the latest satellite–gauge precipitation products and their hydrologic applications over the Huaihe River basin. *J. Hydrol.*, **536**, 302–319, doi: 10.1016/j.jhydrol.2016.02.054.

Tan, M. L., A. L. Ibrahim, Z. Duan, et al., 2015: Evaluation of six high-resolution satellite and ground-based precipitation products over Malaysia. *Remote Sens.*, **7**, 1504–1528, doi: 10.3390/rs70201504.

Tian, Y. D., C. D. Peters-Lidard, and J. B. Eylander, 2010: Real-time bias reduction for satellite-based precipitation estimates. *J. Hydrometeor.*, **11**, 1275–1285, doi: 10.1175/2010JHM1246.1.

Vu, T. T., L. Li, and K. S. Jun, 2018: Evaluation of multi-satellite precipitation products for streamflow simulations: A case study for the Han River basin in the Korean Peninsula, East Asia. *Water*, **10**, 642, doi: 10.3390/w10050642.

Wang, N., W. B. Liu, F. B. Sun, et al., 2020: Evaluating satellite-based and reanalysis precipitation datasets with gauge-observed data and hydrological modeling in the Xihe River Basin, China. *Atmos. Res.*, **234**, 104746, doi: 10.1016/j.atmosres.2019.104746.

Wang, Z. L., R. D. Zhong, C. G. Lai, et al., 2017: Evaluation of the GPM IMERG satellite-based precipitation products and the hydrological utility. *Atmos. Res.*, **196**, 151–163, doi: 10.1016/j.atmosres.2017.06.020.

Wu, H., R. F. Adler, Y. D. Tian, et al., 2014: Real-time global flood estimation using satellite-based precipitation and a coupled land surface and routing model. *Water Resour. Res.*, **50**, 2693–2717, doi: 10.1002/2013WR014710.

Wu, Z. Y., Z. G. Xu, F. Wang, et al., 2018: Hydrologic evaluation of multi-source satellite precipitation products for the upper Huaihe River basin, China. *Remote Sens.*, **10**, 840, doi: 10.3390/rs10060840.

Xu, H. L., C.-Y. Xu, S. D. Chen, et al., 2016: Similarity and difference of global reanalysis datasets (WFD and APHRODITE) in driving lumped and distributed hydrological models in a

humid region of China. *J. Hydrol.*, **542**, 343–356, doi: 10.1016/j.jhydrol.2016.09.011.

Xue, X. W., Y. Hong, A. S. Limaye, et al., 2013: Statistical and hydrological evaluation of TRMM-based Multi-satellite Precipitation Analysis over the Wangchu Basin of Bhutan: Are the latest satellite precipitation products 3B42V7 ready for use in ungauged basins? *J. Hydrol.*, **499**, 91–99, doi: 10.1016/j.jhydrol.2013.06.042.

Yong, B., L.-L. Ren, Y. Hong, et al., 2010: Hydrologic evaluation of Multisatellite Precipitation Analysis standard precipitation products in basins beyond its inclined latitude band: A case study in Laohahe basin, China. *Water Resour. Res.*, **46**, W07542, doi: 10.1029/2009WR008965.

Yong, B., B. Chen, Y. D. Tian, et al., 2016: Error-component analysis of TRMM-based multi-satellite precipitation estimates over mainland China. *Remote Sens.*, **8**, 440, doi: 10.3390/rs8050440.

Yuan, F., L. M. Zhang, K. W. W. Win, et al., 2017: Assessment of GPM and TRMM multi-satellite precipitation products in streamflow simulations in a data-sparse mountainous watershed in Myanmar. *Remote Sens.*, **9**, 302, doi: 10.3390/rs9030302.

Yuan, F., L. M. Zhang, K. M. W. Soe, et al., 2019: Applications of TRMM- and GPM-era multiple-satellite precipitation products for flood simulations at sub-daily scales in a sparsely gauged watershed in Myanmar. *Remote Sens.*, **11**, 140, doi: 10.3390/rs11020140.

Zhang, S. J., D. H. Wang, Z. K. Qin, et al., 2018: Assessment of the GPM and TRMM precipitation products using the rain gauge network over the Tibetan Plateau. *J. Meteor. Res.*, **32**, 324–336, doi: 10.1007/s13351-018-7067-0.

Zhang, Z. X., J. X. Tian, Y. H. Huang, et al., 2019: Hydrologic evaluation of TRMM and GPM IMERG satellite-based precipitation in a humid basin of China. *Remote Sens.*, **11**, 431, doi: 10.3390/rs11040431.

Zhao, F. B., Y. P. Wu, L. J. Qiu, et al., 2018: Parameter uncertainty analysis of the SWAT model in a mountain-loess transitional watershed on the Chinese Loess Plateau. *Water*, **10**, 690, doi: 10.3390/w10060690.

Zhao, R.-J., 1992: The Xinanjiang model applied in China. *J. Hydrol.*, **135**, 371–381, doi: 10.1016/0022-1694(92)90096-E.

Zhong, R. D., X. H. Chen, C. G. Lai, et al., 2019: Drought monitoring utility of satellite-based precipitation products across mainland China. *J. Hydrol.*, **568**, 343–359, doi: 10.1016/j.jhydrol.2018.10.072.

Zhou, Z. H., X. C. Gao, Z. Y. Yang, et al., 2019: Evaluation of hydrological application of CMADS in Jinhua River basin, China. *Water*, **11**, 138, doi: 10.3390/w11010138.

Zhu, Q., X. C. Gao, Y.-P. Xu, et al., 2019: Merging multi-source precipitation products or merging their simulated hydrological flows to improve streamflow simulation. *Hydrol. Sci. J.*, **64**, 910–920, doi: 10.1080/02626667.2019.1612522.

Tech & Copy Editor: Qi WANG